LA-UR-23-29979
Accepted Manuscript

Solid-State Transformation of Uranyl Peroxide Materials through High-Level Irradiation

Rier, Melissa Catherine Fairley
Sigmon, Ginger E.
LaVerne, Jay A.

Provided by the author(s) and the Los Alamos National Laboratory (2024-06-20).

To be published in: Inorganic Chemistry

DOI to publisher's version: 10.1021/acs.inorgchem.3c03373

Permalink to record:
https://permalink.lanl.gov/object/view?what=info:lanl-repo/lareport/LA-UR-23-29979

Los Alamos National Laboratory, an affirmative action/equal opportunity employer, is operated by Triad National Security, LLC for the National Nuclear Security Administration of U.S. Department of Energy under contract 89233218CNA000001. By approving this article, the publisher recognizes that the U.S. Government retains nonexclusive, royalty-free license to publish or reproduce the published form of this contribution, or to allow others to do so, for U.S. Government purposes. Los Alamos National Laboratory requests that the publisher identify this article as work performed under the auspices of the U.S. Department of Energy. Los Alamos National Laboratory strongly supports academic freedom and a researcher's right to publish; as an institution, however, the Laboratory does not endorse the viewpoint of a publication or guarantee its technical correctness.

Solid-state transformation of uranyl peroxide materials through high-level irradiation

Melissa Fairley[1†], Ginger E. Sigmon[2], and Jay A. LaVerne[1,3*]

[1]Radiation Laboratory, University of Notre Dame, Notre Dame, Indiana 46556, United States

[2]Department of Civil and Environmental Engineering and Earth Sciences, University of Notre Dame, Notre Dame, Indiana 46556, United States

[3]Department of Physics and Astronomy, University of Notre Dame, Notre Dame, IN 46556, United States

Irradiation, Uranyl; Peroxides, Carbonates

ABSTRACT: The solid-state transformation of sodium uranyl triperoxide ($Na_4(UO_2)(O_2)_3 \cdot 9H_2O$, NaUT) to sodium uranyl tricarbonate ($Na_4(UO_2)(CO_3)_3$) by radiolysis has been observed for the first time. The exposure of NaUT to 3 MGy gamma irradiation resulted in partial breakdown of the peroxides forming a mixed peroxide and carbonate species. The effects of He ion irradiation on NaUT was also investigated up to 225 MGy using both hydrated argon and dry argon. The complete conversion to the uranyl tricarbonate phase by 56 MGy using hydrated argon, while dry argon did not fully convert showing the importance of water in the system. He-ion irradiated NaUT samples all convert to the tricarbonate phase with time in air post radiation exposure. This transition was monitored via Raman spectroscopy, infrared spectroscopy (IR), and powder X-ray diffraction (PXRD) to further confirm the identity of the final product as the sodium uranyl tricarbonate, čejkaite. This transformation outlines a mechanism for the mobility of uranyl in natural environments and in the Hanford tanks.

INTRODUCTION

The fundamental understanding of uranyl materials response to radiation is crucial for nuclear waste systems, transport of uranium in the environment, and transformations of uranium materials.[1-3] Uranyl tricarbonate minerals have been discovered around the world.[4-5] Secondary uranyl carbonate phases have also been found on the Chernobyl "lava", in the Hanford waste tanks, and on commercial spent nuclear fuel.[6-9]

Peroxide is used throughout the fuel cycle as an oxidant to convert U(IV) to U(VI).[10] Uranyl peroxide chemistry has been studied in depth across the pH range.[11-12] At lower pH the uranyl minerals studtite and metastudtite form, while at higher pH phases uranyl peroxide nanoclusters form in the presence of charge balancing countercations.[1] Studtite consists of a chain of uranyl peroxide polyhedra and the nanoclusters are composed of multiple uranyl peroxide polyhedral depending on the size of the cluster.[13] For example, U_{60} contains sixty uranyl peroxide polyhedral bonded together through peroxide and hydroxide edges. Individual polyhedra have been isolated to form uranyl triperoxide monomers (UT) containing three terminal peroxide units (Figure 1a) in the equatorial plane.[14-16] Recently, the first uranyl superoxide compound was reported and found to age in solution to a mixed uranyl peroxo-carbonate phase, $K_4[UO_2(CO_3)_2(O_2)] \cdot H_2O$, and further into a uranyl tricarbonate compound, $K_3Na[UO_2(CO_3)_3] \cdot H_2O$.[2] The aging of the uranyl superoxide in atmospheric conditions produced the same uranyl peroxo-carbonate compound after six days.[2] Solution studies showed that the uranyl peroxo-carbonate complexes also decompose to uranyl tricarbonate species (Figure 1b).[17] Uranyl tricarbonate phases have been discovered and characterized in nature as well as synthesized in a laboratory setting.[4]

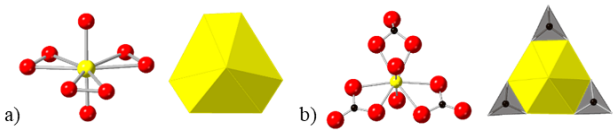

Figure 1) Ball and stick (left) and polyhedral representation (right) of (a) $Na_4(UO_2)(O_2)_3 \cdot 9H_2O$ and (b) $Na_4(UO_2)(CO_3)_3$.

Irradiations with both gamma-rays and He-ions allow materials to be studied under extreme conditions similar to nuclear waste streams and in some environmental systems. Uranyl peroxide nanoclusters and studtite are fairly stable under γ-irradiation and begin to form an unstable uranyl peroxide when exposed to intense He-ion irradiation.[3] Irradiation of studtite in different aqueous systems relevant to the open environment has also been explored.[18] Isolated uranyl triperoxide polyhedral with Li and Ca counter cations (LiUT and CaUT salts) have been studied with gamma irradiation revealing the ionization of the terminal peroxide group(s)[19] while in solution LiUT forms a uranyl peroxide cage cluster (U_{24}) at lower doses and higher doses forms a uranyl oxyhydroxide sheet structure.[20]

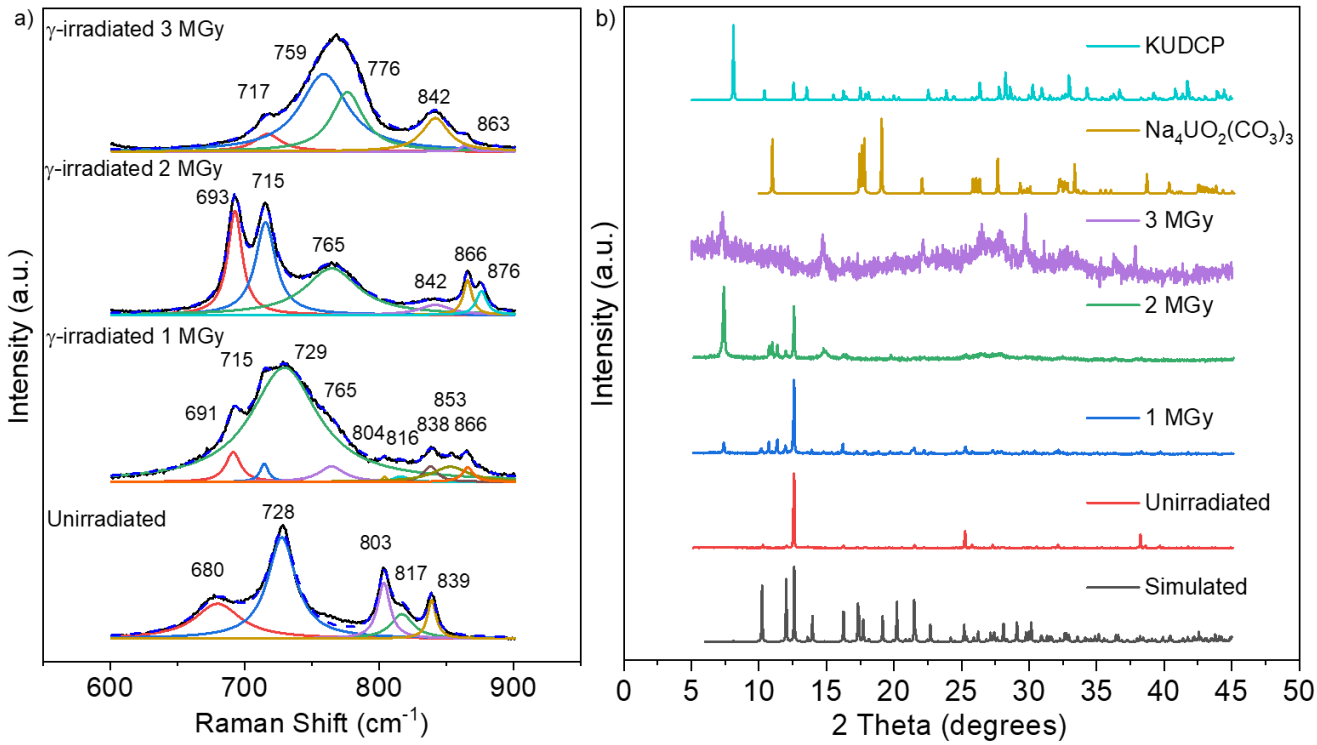

Figure 2. Gamma-irradiation of NaUT to 1 MGy, 2 MGy, and 3 MGy. a) Raman spectroscopy and b) PXRD patterns with simulated $Na_4UO_2(CO_3)_3$ (04-020-1008)[21] and KUDCP (04-011-9445).[22]

In this study we examine the NaUT salt up to 3MGy with γ-irradiation and up to 225 MGy of He-ion irradiation in the presence and absence of H_2O. We follow the solid-state transformation of this material via vibrational (Raman and infrared) spectroscopy and powder X-ray diffraction.

RESULTS AND DISCUSSION

Gamma-irradiation:

The experimental data for unirradiated NaUT and gamma irradiated NaUT to 1, 2, and 3 MGy are displayed in Figure 2. Gamma irradiations were performed with degassed samples, but exposed to air for spectroscopic analysis. Further details of sample preparation can be found in the Methods and Supplementary Information. The Raman spectra of the unirradiated NaUT aligns with previously reported spectra (Figure 2a). The stretch at 728 cm^{-1} is attributed to the symmetric uranyl stretch (ν_1 UO_2^{2+}) while the bands at 680, 803, 817, and 839 cm^{-1} are due to the terminal peroxo stretches ($\nu_{1\text{-}3}$ O-O).[23] Upon radiolysis of the material to 1 MGy, multiple peaks appear and shifts to the uranyl and peroxide units suggest a transition to a new phase. These new peaks start to align with the addition of carbonate to the structure. At 1MGy, there is a mixture of the NaUT and a sodium uranyl dicarbonate peroxide phase (NaUDCP). The peaks at 729, 804, 816, and 838 cm^{-1} are attributed to the NaUT[23] while the peaks at 691, 715, 765, 853, and 866 cm^{-1} are attributed to the new NaUDCP phase.[2] As we continue to 2 MGy and 3 MGy of gamma irradiation, the NaUT character of the material continues to disappear and the phase has mostly converted to NaUDCP. The NaUCDP material matches that of previously described examples of a K-uranyl dicarbonate peroxide phase.[2] The peaks become broader due to the material losing its crystallinity as the phase is changing in the solid state. This conversion does not produce a uniform material throughout the irradiation as displayed in Figure S1. Particle sizes vary and conversion likely occurs at different rates on the surface compared to the bulk.

The diffractogram of the unirradiated NaUT is in agreement with the simulated powder pattern from the crystal structure (Figure 2b). At 1 MGy, the sample resembles the unirradiated material with minor changes starting to occur specifically with new diffraction peaks appearing at 7.3˚, 10.6˚, 10.8˚, and 11.2˚ two-theta. At 2 MGy, we start to see larger changes and a shift to a new material with minor amounts of NaUT remaining. Several of the new diffraction peaks are similar to that of a reported $K_4[UO_2(O_2)(CO_3)_2]\cdot 2.5\ H_2O$ (KUDCP)[22] and sodium uranyl tricarbonate, $Na_4(UO_2)(CO_3)_3$ (Figure 2b).[21] By 3 MGy of gamma irradiation, potentially many phases are present including an amorphous phase (Figure 2b). Infrared spectra were also collected (Figure S4) and agree with the Raman spectroscopy.

Gamma radiolysis was performed with flame sealed samples that had been previously outgassed by vacuum. There was not enough residual carbon to give the carbonates observed here. A reasonable conclusion is that an unstable uranyl peroxide, perhaps a radical, is formed in radiolysis that is persistent enough to react with carbon dioxide when the sample is exposed to air for spectral analysis.

He-ion irradiation:

To obtain higher doses of irradiation, He-ion irradiation was utilized. Hydrated argon gas was flowed over the samples to prevent dehydration and interaction with O_2 during irradiation. Raman, IR, and PXRD were used to track the solid-state transformation of the material.

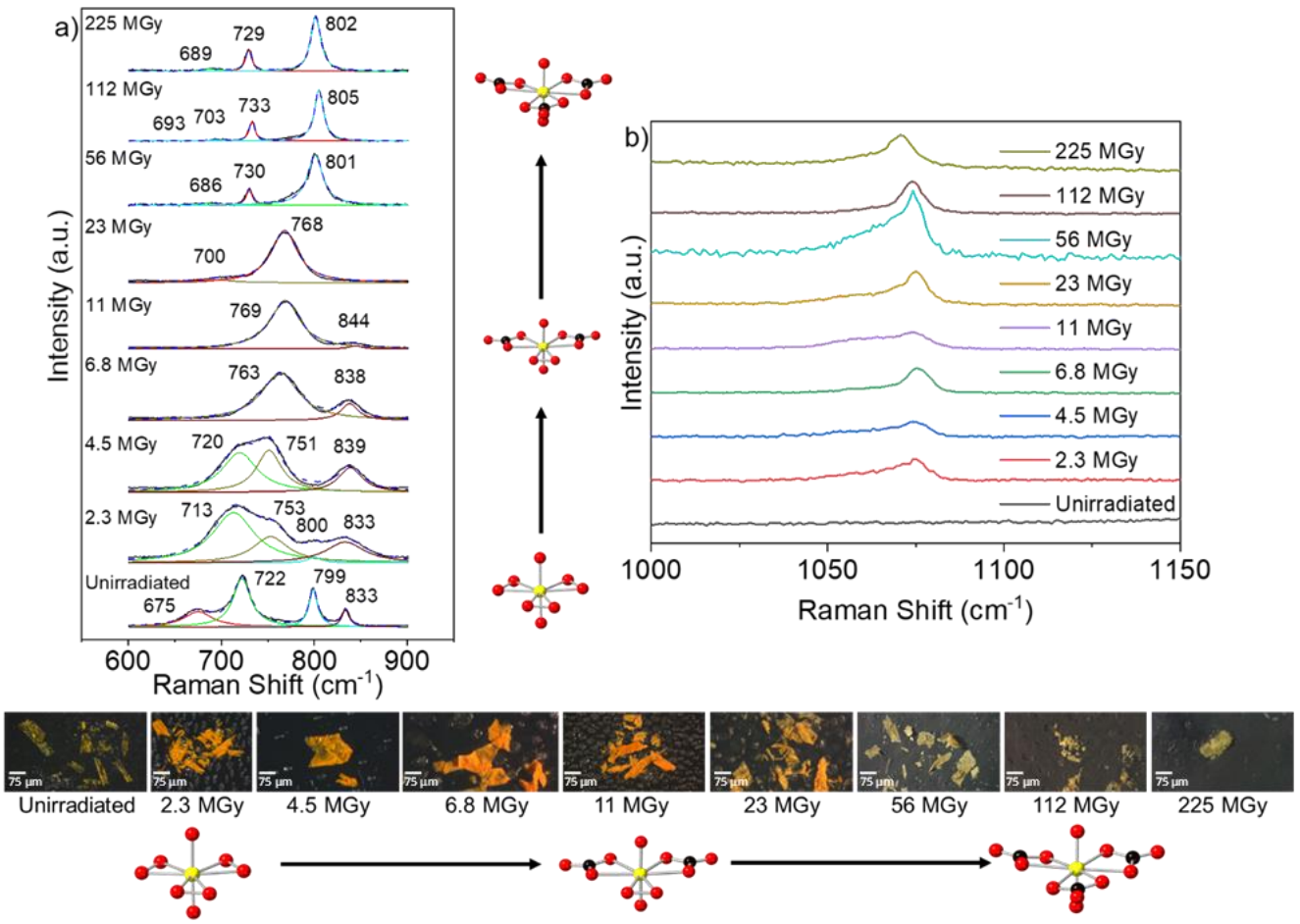

Figure 3. Raman spectra of unirradiated NaUT and He-ion irradiated NaUT using hydrated Ar (2.3- 225 MGy). a) uranyl region and b) carbonate region. The lower bar shows consecutive SEM snapshots at each stage of the radiolysis with He-ions.

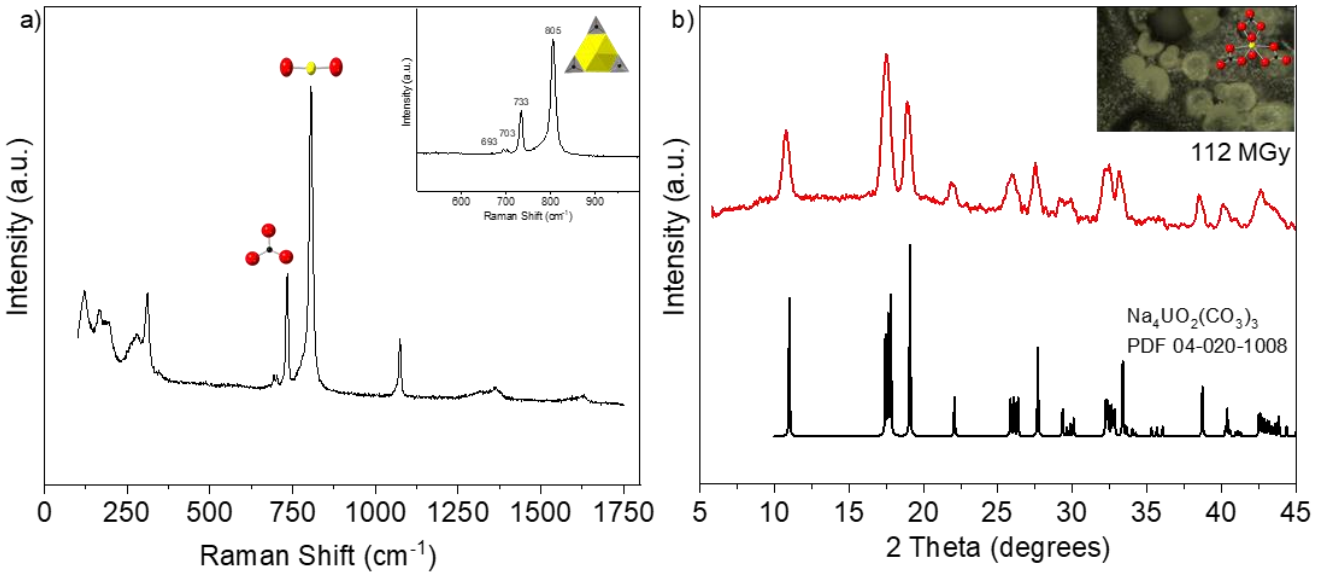

Figure 4. a) Extended Raman spectra of He-ion irradiated NaUT using hydrated Ar (112 MGy) and b) Powder X-ray diffraction of He-ion irradiated NaUT using hydrated Ar (112 MGy).

Figure 3 displays the Raman spectra obtained from unirradiated and He-ion irradiated NaUT up to 225 MGy with corresponding microscope images of the irradiated samples. Upon 2.3 MGy of irradiation, there is a visible color change in the material from a clear yellow-orange crystal to a cloudy orange. The stretches at 720 cm^{-1} (CO_3^{2-}), 751 cm^{-1} (ν_1 UO_2^{2+} bound to CO_3^{2-}), and 839 cm^{-1} (O-O) suggest in-growth of a uranyl carbonate peroxide

phase.[2] The 2.3 and 4.5 MGy levels of irradiation suggest transition phases between the triperoxide phase ($Na_4(UO_2)(O_2)_3 \cdot 9H_2O$) to the NaUDCP phase ($Na_4(UO_2)(O_2)(CO_3)_2$) are present. These transitions are in good alignment with the gamma irradiations to 3 MGy. At 4.5 MGy of irradiation, the uranyl stretches continues to blue shift indicating shortening of the uranyl bond. A change in the chemical environment of the uranyl ion such as the breaking or replacing of one peroxide group in the equatorial plan is plausible for this shift.

By 6.8 MGy, the only phase present is the NaUDCP with bands at 763 and 838 cm^{-1} corresponding to the uranyl ion bound to two CO_3^{2-} and one peroxo and peroxide bound to the uranyl ion, respectively. Peaks are broader due to the material losing its crystallinity and changing form in the solid state. Similar phases were previously described in $K_4(UO_2)(O_2)(CO_3)_2 \cdot H_2O$ indicating two of the terminal peroxide groups have been replaced by carbonate.[2, 24] It is likely the terminal peroxide groups were ionized forming an unstable species for which, when exposed to air, CO_3^{2-} rapidly displaces. With continued irradiation, these stretches remain prominent until 23 MGy of He-ion irradiation when the peroxo stretch at 838 cm^{-1} is no longer present. The 768 cm^{-1} (ν_1 UO_2^{2+} bound to CO_3^{2-}) peak is indicative of a uranyl carbonate phase with no remaining peroxo and the stretch at 700 cm^{-1} represents carbonate bound to the uranyl.[17, 25]

Upon irradiation to 56 MGy, a second visible color change occurs from cloudy orange and to a cloudy pale yellow, and the Raman stretches split to 686, 730, and 801 cm^{-1}. At this point, the peaks are starting to become sharper as the material is starting to recrystallize as a stable phase. At 112 MGy, the material has sharp peaks at 693, 703, 733, and 805 cm^{-1}. The band at 805 cm^{-1} is attributed to UO_2^{2+}, while the stretches at 693, 703, and 733 cm^{-1} are assigned to bidentate CO_3^{2-}. The stretch at 1074 cm^{-1} due to the CO_3^{2-} is shown in Figure 3b and in the extended scans (Figure S6). Similar peak positions are found in the sample irradiated to 225 MGy. These Raman assignments align with the previously reported spectra for the natural specimen of $Na_4(UO_2)(CO_3)_3$, čejkaite.[26] Figure 4a displays the extended Raman spectra for NaUT irradiated to 112 MGy where all bands are associated with the sodium uranyl tricarbonate. Variability in static Raman spectra is displayed in Figure S5. Extended and fitted Raman spectra for all doses are displayed in Figure S6 and Figure S7, respectively.

This conversion was also tracked using IR presented in Figure S8. At 56 MGy, all of the stretches are associated with the sodium uranyl tricarbonate mineral agreeing with the Raman spectroscopy. Specifically, the UO_2^{2+} antisymmetric stretching at 845 cm^{-1}, the CO_2^{2-} out of plane bending at 829 cm^{-1} overlapping with UO_2^{2+} symmetric stretches while the in-plane bending is observed between 620-735 cm^{-1}, CO_2^{2-} symmetric stretching at 1062 cm^{-1}, the double degenerate CO_2^{2-} antisymmetric stretching vibrations at 1339 and 1556 cm^{-1}.[26] The splitting of the latter suggest the carbonate groups are bonded in a bidentate fashion in the equatorial plane.[26-27] The stretches present remain consistent through 225 MGy. The

The PXRD analysis of NaUT irradiated to 112 MGy shows no remaining NaUT, but rather the diffractogram matches the simulated pattern for natural $Na_4(UO_2)(CO_3)_3$ (Figure 4b).[21] Powder patterns obtained from He-ion irradiated NaUT with 6.8 MGy, 23 MGy, and 112 MGy are displayed in Figure S9. This shows the transition of the NaUT goes through less crystalline and amorphous phases to produce crystalline čejkaite through a solid-state transition. The formation of čejkaite from the radiolysis of humid solid uranyl peroxide is different from that found for the radiolysis of aqueous solutions of uranyl peroxide with added hydrogen peroxide and carbonate.[18] In that study studtite and meta-schoepite were formed depending on the pH.

A He-ion irradiation dose study was also completed using a dry argon flow over the sample. This revealed a similar transformation of transition phases up to 23 MGy but did not form the $Na_4(UO_2)(CO_3)_3$ at higher doses. For doses of 23 MGy up to 225 MGy under dry argon flow, the sample remained a uranyl carbonate phase[19] with a single peak at 777 cm^{-1} (Figure S10 and S11). The transformation under dry argon was also tracked utilizing IR (Figure S12).

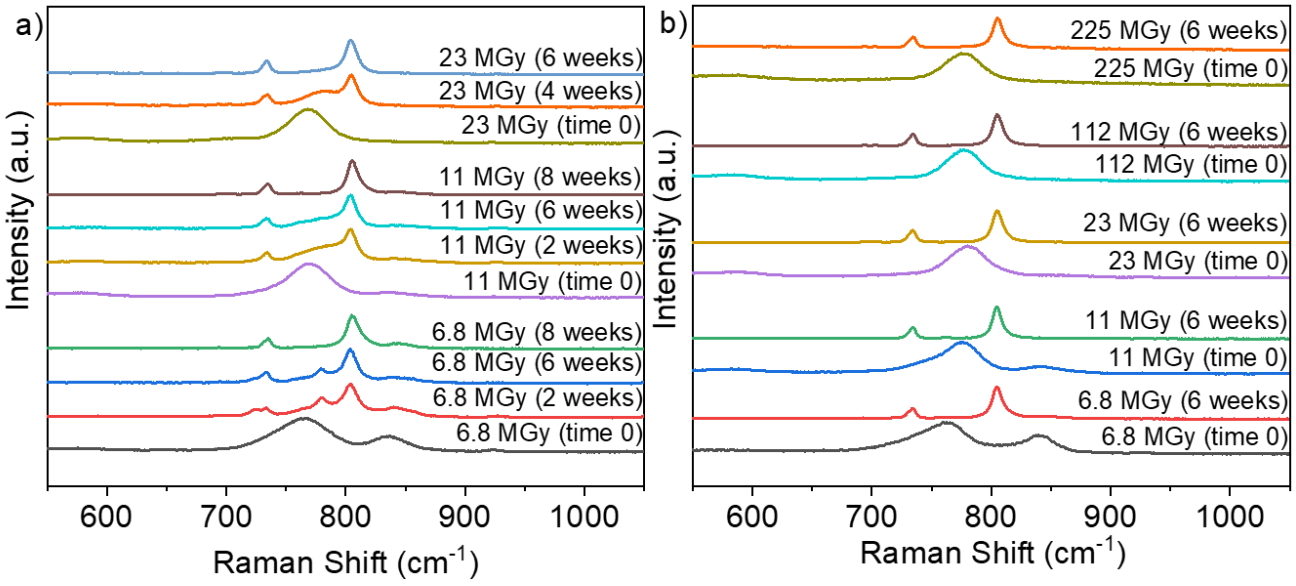

Figure 5. Raman spectra of a) aged hydrated Ar He-ion irradiated NaUT (6.8-23 MGy) and b) aged dry Ar He-ion irradiated NaUT (6.8-225 MGy).

Aged Study:

Recent studies have shown additional information can be gained from aging the material.[2, 19] Samples of NaUT irradiated to 6.8, 11, and 23 MGy via He-ion (with hydrated Ar flow) were monitored up to eight weeks while exposed to ambient conditions (Figure 5a). After just two weeks, the 6.8 and 11 MGy samples have stretches at 733 and 805 cm^{-1} attributed to the $Na_4(UO_2)(CO_3)_3$, and are fully converted by eight weeks. These aged samples also have stretches 723 and 780 cm^{-1} potentially due to other mixed peroxo-carbonate phases.[2] The 23 MGy NaUT sample is fully converted to the $Na_4(UO_2)(CO_3)_3$ after six weeks.

The samples of NaUT irradiated via He-ion and dry argon flow show similar results. The 6.8 MGy and 11 MGy samples have two main peaks that fully converted to $Na_4(UO_2)(CO_3)_3$ after six weeks. The 23 MGy, 112 MGy, and 225 MGy samples have also fully converted to $Na_4(UO_2)(CO_3)_3$ after six weeks.

CONCLUSION

Čejkaite is an important sodium uranyl carbonate mineral that has been found both on the Chernobyl lava[6] and in the Hanford tanks.[7-8] The Hanford tanks have čejkaite as a major phase in the crust. Čejkaite was formed from the interaction of carbon dioxide in the air with the uranium in the sludge.[9] The solid-state transformation of the NaUT to čejkaite via irradiation in the current study suggests that if uranyl peroxide phases are present and experience irradiation, they will convert to carbonate species. We hypothesize the terminal peroxide forms an unstable species upon irradiation, which is replaced by CO_3^{2-} rapidly when exposed to air. These results further suggest that uranyl peroxide species may potentially be more prominent in the environment but convert to the carbonate species that are commonly discovered. [5]

The formation of carbonates has been observed when uranyl super-oxides are exposed to air, though to our knowledge it has not been reported from a uranyl peroxide previously.[2, 28] Further work will have to determine if the mechanisms are the same. Recent thermodynamic data shows uranyl carbonate minerals are more thermodynamically stable than peroxide phases.[29] This aligns well with the radiation-promoted transformation from the triperoxide to the tricarbonate phase. In the case of the superoxide compound, the superoxide converted to the $(UO_2)(O_2)(CO_3)_2^{4-}$ phase in six days. With He-ion irradiation, this was done in a matter of minutes as well as the full conversion to the tricarbonate phase at and above 56 MGy.

The solid-state transformation is a direct 1:1 change from a triperoxide phase ($Na_4(UO_2)(O_2)_3$) to a tricarbonate phase ($Na_4(UO_2)(CO_3)_3$). The presence of the water in the hydrated Ar flow during irradiation may play a role in the rate of transformation. Upon irradiation with 56 MGy, the final species formed directly, while over time all irradiated samples converted to the $Na_4(UO_2)(CO_3)_3$ phase. The dry Ar flow samples eventually formed the final tricarbonate species but the final conversion to $Na_4(UO_2)(CO_3)_3$ took longer to occur with aging of the samples post-irradiation. Once the triperoxide is activated, the reaction will continue until it reaches the tricarbonate phase. The dry argon flow could lead to a different path to the final product with the absence of water on the surface of the material. The role of the water is not yet understood, but it must couple with the unstable peroxide formed in radiolysis. In nuclear waste and environmental systems, H_2O will be readily available therefore it is important to explore systems with and without it present.

We will continue to examine other uranyl peroxide and uranyl (oxy)hydrate phases to see how they behave when exposed to irradiation environments and if they lead to tricarbonate phases. Water is prominent in many applications where uranium is found, therefore, it is important to understand its role in irradiation schemes. The exploration of radiation effects on uranyl peroxides is a promising area to expand the fundamental understanding of their transport in the environment and nuclear waste systems.

EXPERIMENTAL METHODS

Synthesis of NaUT. Uranyl nitrate hexahydrate ($UO_2(NO_3)_2{\cdot}6H_2O$, 0.5 M, 1 mL), hydrogen peroxide (H_2O_2, 30%, 1 mL), and sodium hydroxide (NaOH, 5M, 3 mL) were combined in a glass scintillation vial. After two minutes, crystals of the NaUT begin to form and precipitate from solution. The crystals were harvested via vacuum filtration and placed in a capped glass vial in the refrigerator.

Characterization of NaUT. Raman and infrared (IR) spectroscopy were used to characterize the material before and after irradiation. Powder X-ray Diffraction (PXRD) was used to confirm there were no impurities present within the starting material. Single crystal X-ray diffraction (SCXRD) was used to collect powder diffraction on small amounts of materials of the irradiated NaUT.

Raman spectroscopy measurements were collected using a Renishaw inVia Raman instrument with an excitation laser of 785 nm and an estimated spot size of 10 nm. Static scans were collected using 0.1% laser power, 5 second exposure time, and 30 accumulations. Extended scans were performed from 100-1200 cm^{-1}, with a 0.1% laser power, 10 second exposure time, and 15 accumulations. Cosmic ray removal was done for all Raman spectra. OriginPro and Lorentzian functions were utilized to fit all Raman spectra.[30] We note the fittings for the spectra obtained from 1 MGy γ-irradiated NaUT sample needed one parameter to be fixed. The fitting was completed with no restraints followed by restraining the 853 cm^{-1} stretch due to dependency values close to 1. The fitting parameters are found in Table S1 and S2.

Infrared spectra were collected using Bruker Lumos FT-IR in the attenuated total reflectance (ATR) mode. The spectral range collected was from 600-3998 cm^{-1}. The spectra are an accumulation of 64 scans and with a resolution of 4 cm^{-1}.

PXRD measurements of γ-irradiated samples were collected using a Bruker D8 Advance Davinci powder X-ray diffractometer equipped with a Cu Kα X-ray source. Diffractograms were collected from 5-45˚ 2 theta, with 0.02˚ scan step and 3 seconds count time per step while the sample was rotated at 15 rpm. For He-ion irradiated samples, PXRD patterns were collected using a Bruker Quazar single crystal X-ray diffractometer with monochromated Mo-Kα radiation. A few single crystals were mounted to the tip of a glass fiber using epoxy. Diffractograms were collected from 5-45˚ 2 theta.

Irradiation. Gamma irradiation experiments were completed using a self-enclosed Shepherd ^{60}Co source housed in the University of Notre Dame Radiation Laboratory. The dose rate was determined by Fricke dosimetry to be about 88.4 Gy/min and corrected for natural decay. Crystals of NaUT (about 100 micrograms per sample) were degassed for gamma irradiation using a freeze-pump-thaw technique and flame sealed in Pyrex tubes (1 cm diameter by 10 cm long). Gamma irradiation dose studies were completed from 1-3 MGy cumulative dose. For

He-ion irradiations, 5 MeV He-ions were applied with a beam current of about 20 nA using the 9S Accelerator in the Nuclear Science Laboratory at the University of Notre Dame. Absolute dosimetry was completed by combining the incident energy and integrated beam current. The diameter of the beam is approximately 0.635 cm with a penetration of approximately of 23 μm estimated by SRIM/TRIM.[31] The doses for He-ion irradiation ranged from 2.3 to 225 MGy with a dose rate of about 2.5 MGy/min. Beam current was limited to about 25 nA to avoid heating. Measured temperature of the backing substrate rose only about 2 °C with the beam on. Hydrated or dehydrated Ar was flowed over the sample surface to prevent oxygen interaction during irradiation. Hydration was achieved by first bubbling the Ar through a water reservoir to remove any air and carbonates.

ASSOCIATED CONTENT

Raman spectra, Raman spectra fittings, Infrared spectra, and powder X-ray diffraction (PDF) This material is available free of charge via the Internet at http://pubs.acs.org.

AUTHOR INFORMATION

Corresponding Author

*Jay.A.LaVerne.1@nd.edu

Present Addresses

†Materials Synthesis and Integrated Devices MPA-11, Los Alamos National Laboratory, Los Alamos, New Mexico 87545, United States

Author Contributions

M.F. and G.S. conceived this work and J.L directed the team. M.F. and G.S. designed the experiments and prepared the manuscript. All authors discussed and contributed to the manuscript at all stages.

Funding Sources

This work was supported by Department of Energy, National Nuclear Security Administration, under Award Number DE-NA0003763.

Notes

The authors declare no competing financial interests.

ACKNOWLEDGMENT

The authors acknowledge the Center for Sustainable Energy at Notre Dame (ND Energy) Materials Characterization Facility for the use of the Bruker D8 Advance Davinci powder X-ray diffractometer. The authors thank Prof. Michael Wiescher for making available the facilities of the Notre Dame Nuclear Science Laboratory, which is supported by the U.S. National Science Foundation through Grant Phys-0758100, and Prof. Ian Carmichael for making available the facilities of the Notre Dame Radiation Laboratory, which is supported by DOBES through Grant DE-FC02-04ER15533. This contribution is NDRL-5408 from the Notre Dame Radiation Laboratory.

REFERENCES

(1) Burns, P. C.; Ewing, R. C.; Navrotsky, A., Nuclear Fuel in a Reactor Accident. *Science* **2012,** *335*, 1184-1188.

(2) Kravchuk, D. V.; Dahlen, N. N.; Kruse, S. J.; Malliakas, C. D.; Shand, P. M.; Forbes, T. Z., Isolation and Reactivity of Uranyl Superoxide. *Angew. Chem., Int. Ed.* **2021,** *60*, 15041-15048.

(3) Fairley, M.; Myers, N. M.; Szymanowski, J. E. S.; Sigmon, G. E.; Burns, P. C.; LaVerne, J. A., Stability of Solid Uranyl Peroxides under Irradiation. *Inorg. Chem.* **2019,** *58*, 14112-14119.

(4) Clark, D. L.; Hobart, D. E.; Neu, M. P., Actinide Carbonte Complexes and Their Importance in Actinide Environmental Chemistry. *Chem. Rev.* **1995,** *95*, 25-48.

(5) Gurzhiy, V. V.; Kalashnikova, S. A.; Kuporev, I. V.; Plášil, J., Crystal Chemistry and Structural Complexity of the Uranyl Carbonate Minerals and Synthetic Compounds. *Crystals* **2021,** *11*, 704.

(6) Burakov, B. E.; Strykanova, E. E.; Anderson, E. B., Secondary Uranium Minerals on the Surface of Chernobyl "Lava". *MRS Online Proc. Libr.* **2012,** *465*, 1309.

(7) Cantrell, K. J.; Krupka, K. M.; Deutsch, W. J.; Lindberg, M. J., Residual Waste from Hanford Tanks 241-C-203 and 241-C-204. 2. Contaminant Release Model. *Environ. Sci. Technol.* **2006,** *40*, 3755-3761.

(8) Krupka, K. M.; Schaef, H. T.; Arey, B. W.; Heald, S. M.; Deutsch, W. J.; Lindberg, M. J.; Cantrell, K. J., Residual Waste from Hanford Tanks 241-C-203 and 241-C-204. 1. Solids Characterization. *Environ. Sci. Technol.* **2006,** *40*, 3749-3754.

(9) Page, J. S.; Reynolds, J. G.; Ely, T. M.; Cooke, G. A., Development of a carbonate crust on alkaline nuclear waste sludge at the Hanford site. *J. Hazard. Mater.* **2018,** *342*, 375-382.

(10) Edwards, C. R.; Oliver, A. J., Uranium processing: A review of current methods and technology. *JOM* **2000,** *52*, 12-20.

(11) Burns, P. C., Nanoscale uranium-based cage clusters inspired by uranium mineralogy. *Mineral. Mag.* **2011,** *75*, 1-25.

(12) Burns, P. C.; Nyman, M., Captivation with Encapsulation: A Dozen Years of Exploring Uranyl Peroxide Capsules. *Dalton Trans.* **2018,** *47*, 5916-5927.

(13) Burns, P. C.; Hughes, K.-A., Studtite, $[(UO_2)(O_2)(H_2O)_2](H_2O)_2$: The First Structure of a Peroxide Mineral. *Am. Mineral.* **2003,** *88*, 1165-1168.

(14) Kubatko, K.-A.; Forbes, T. Z.; Klingensmith, A. L.; Burns, P. C., Expanding the Crystal Chemistry of Uranyl Peroxides: Synthesis and Structures of Di- and Triperoxodioxouranium(VI) Complexes. *Inorg. Chem.* **2007,** *46*, 3657-3662.

(15) Alcock, N. W., The Crystal and Molecular Structure of Sodium Uranyl Triperoxide. *J. Chem. Soc. A* **1968**, 1588-1594.

(16) Nyman, M.; Rodriguez, M. A.; Campana, C. F., Self-Assembly of Alkali-Uranyl-Peroxide Clusters. *Inorg. Chem.* **2010,** *49*, 7748-7755.

(17) Kim, K.-W.; Lee, K.-Y.; Chung, D.-Y.; Lee, E.-H.; Moon, J.-K.; Shin, D.-W., Evaluation of the stability of uranyl peroxo-carbonato complex ions in carbonate media at different temperatures. *J. Hazard. Mater.* **2012,** *233-234*, 213-218.

(18) Li, J.; Maier, A. C.; Jonsson, M., Stability of Studtite in Aqueous Suspension: Impact of HCO^{3-} and Ionizing Radiation on the Dynamics of Dissolution. *ACS Appl. Energy Mater.* **2020,** *3*, 352-357.

(19) Fairley, M.; Felton, D. E.; Sigmon, G. E.; Szymanowski, J. E. S.; Poole, N. A.; Nyman, M.; Burns, P. C.; LaVerne, J. A., Radiation-Induced Solid-State Transformations of Uranyl Peroxides. *Inorg. Chem.* **2022,** *61*, 882-889.
(20) Felton, D. E.; Fairley, M.; Arteaga, A.; Nyman, M.; LaVerne, J. A.; Burns, P. C., Gamma-Ray-Induced Formation of Uranyl Peroxide Cage Clusters. *Inorg. Chem.* **2022,** *61*, 11916-11922.
(21) Li, Y.; Krivovichev, S. V.; Burns, P. C., The crystal structure of $Na_4(UO_2)(CO_3)_3$ and its relationship to schröckingerite. *Mineral. Mag.* **2018,** *65*, 297-304.
(22) Zehnder, R. A.; Peper, S. M.; Scott, B. L.; Runde, W. H., Tetrapotassium dicarbonatodioxoperoxouranium(VI) 2.5-hydrate, $K_4[U(CO_3)_2O_2(O_2)].2.5H_2O$. *Acta Crystallogr., Sect. C: Struct. Chem.* **2005,** *61*, i3-i5.
(23) Dembowski, M.; Bernales, V.; Qiu, J.; Hickam, S.; Gaspar, G.; Gagliardi, L.; Burns, P. C., Computationally-Guided Assignment of Unexpected Signals in the Raman Spectra of Uranyl Triperoxide Complexes. *Inorg. Chem.* **2017,** *56*, 1574-1580.
(24) Goff, G. S.; Brodnax, L. F.; Cisneros, M. R.; Peper, S. M.; Field, S. E.; Scott, B. L.; Runde, W. H., First Identification and Thermodynamic Characterization of the Ternary U(VI) Species, $UO_2(O_2)(CO_3)_2^{4-}$, in UO_2–H_2O_2–K_2CO_3 Solutions. *Inorg. Chem.* **2008,** *47*, 1984-1990.
(25) Kim, K.-W.; Jung, E.-C.; Lee, K.-Y.; Cho, H.-R.; Lee, E.-H.; Chung, D.-Y., Evaluation of the Behavior of Uranium Peroxocarbonate Complexes in Na–U(VI)–CO_3–OH–H_2O_2 Solutions by Raman Spectroscopy. *J. Phys. Chem. A* **2012,** *116*, 12024-12031.
(26) Čejka, J.; Sejkora, J.; Plášil, J.; Bahfenne, S.; Palmer, S. J.; Frost, R. L., Raman spectroscopic study of the uranyl carbonate mineral čejkaite and its comparison with synthetic trigonal $Na_4[UO_2(CO_3)_3]$. *J. Raman Spectrosc.* **2010,** *41*, 459-464.
(27) Čejka, J., Infrared spectroscopy and thermal analysis of the uranyl minerals. *Reviews in Mineralogy and Geochemistry* **1999,** *38*, 521-622.
(28) Kravchuk, D. V.; Forbes, T. Z., Thermodynamics and Chemical Behavior of Uranyl Superoxide at Elevated Temperatures. *ACS Materials Au* **2021**.
(29) Colmenero, F., Thermodynamic properties of the uranyl carbonate minerals roubaultite, fontanite, widenmannite, grimselite, čejkaite and bayleyite. *Inorg. Chem. Front.* **2020,** *7*, 4160-4179.
(30) Lu, G.; Haes, A. J.; Forbes, T. Z., Detection and Identification of Solids, Surfaces, and Solutions of Uranium using Vibrational Spectroscopy. *Coord. Chem. Rev.* **2018,** *374*, 314-344.
(31) Ziegler, J. F.; Ziegler, M. D.; Biersack, J. P., SRIM – The Stopping and Range of Ions in Matter *Nucl. Instrum. Methods Phys. Res., Sect. B* **2010,** *268*, 1818-1823.

Synopsis

The solid-state transformation of sodium uranyl triperoxide monomer, $[UO_2(O_2)_3]^{4-}$, to sodium uranyl tricarbonate, $[UO_2(CO_3)_3]^{4-}$, induced by irradiation was investigated. The exposure of NaUT to gamma irradiation resulted in mixed peroxide carbonate species while at higher doses of He-ion irradiation with hydrated argon the complete transformation to the uranyl tricarbonate phase was viewed. He-ion irradiations with dry argon did not fully convert to the uranyl tricarbonate suggesting the importance in water of the system.

Table of Contents Graphic

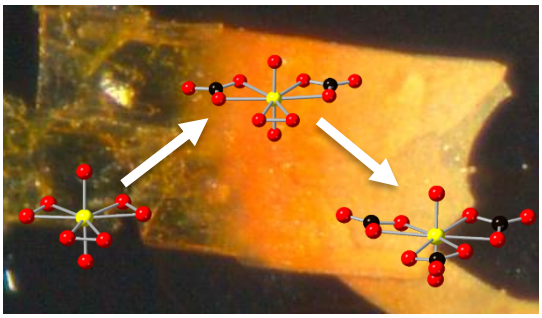

Solid-state transformation of uranyl peroxide materials through high-level irradiation

Melissa Fairley[1], Ginger E. Sigmon[2], and Jay A. LaVerne[3*]

1 - Radiation Laboratory, University of Notre Dame, Notre Dame, Indiana 46556, United States
2 - Department of Civil and Environmental Engineering and Earth Sciences, University of Notre Dame, Notre Dame, Indiana 46556, United States
3 - Department of Physics, University of Notre Dame, Notre Dame, IN 46556, United States
* - corresponding author, Jay.A.LaVerne.1@nd.edu

TABLE OF CONTENTS

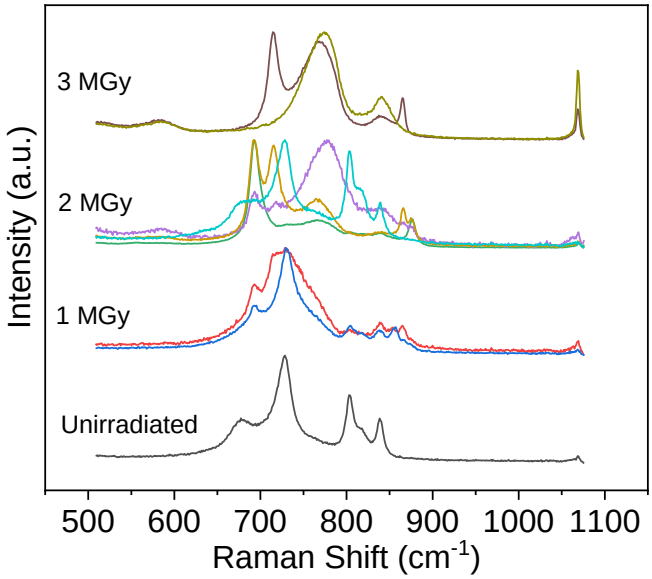

Figure S1. Static Raman spectra obtained from unirradiated and gamma-irradiated NaUTP (1 MGy-3 MGy). Multiple lines at the same dose indicate different particles of the sample.

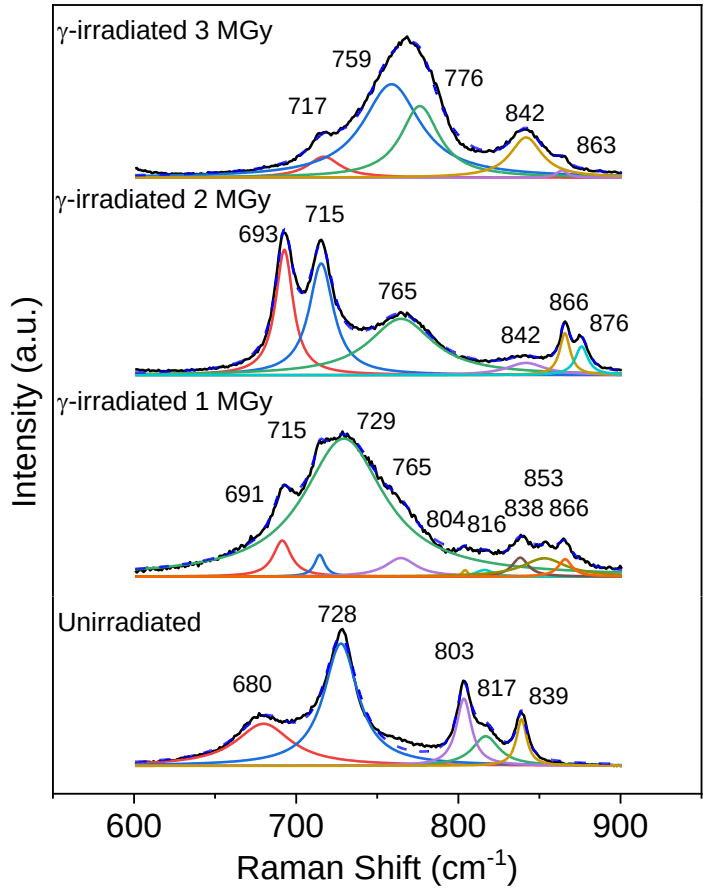

Figure S2. Fitted Raman spectra for unirradiated NaUT, γ-irradiated NaUT 1MGy-3 MGy with the raw data in black and fit in dashed blue.

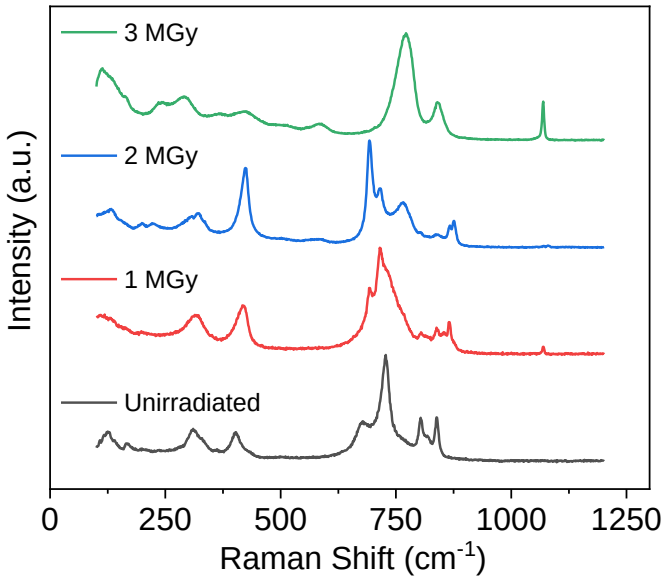

Figure S3. Extended Raman spectra obtained from unirradiated and gamma-irradiated NaUTP (1 MGy-3 MGy).

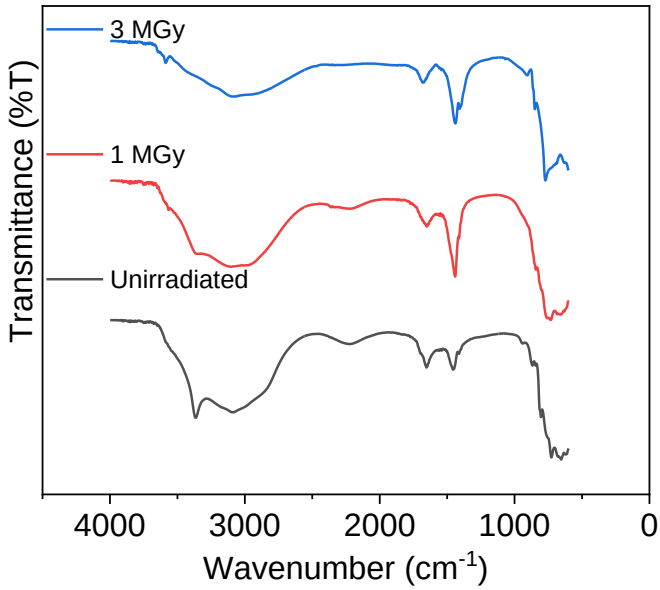

Figure S4. IR spectra obtained from unirradiated and gamma-irradiated NaUT (1 MGy and 3 MGy).

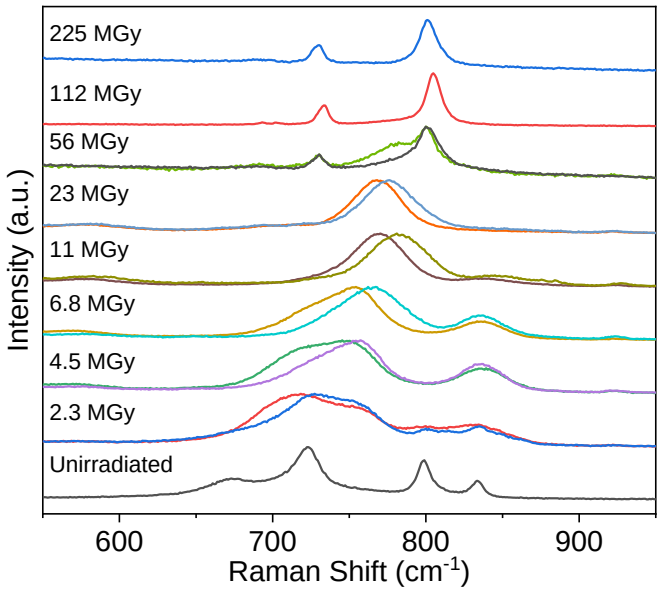

Figure S5. Static Raman spectra obtained from unirradiated and He-ion irradiated NaUT using hydrated Ar (2.3 MGy-225 MGy). Multiple lines at the same dose indicate different particles of the sample.

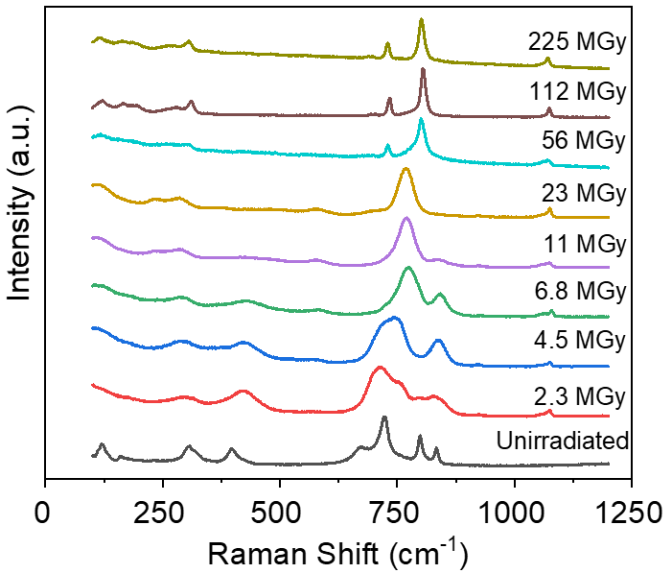

Figure S6. Extended Raman spectra obtained from unirradiated and He-ion irradiated NaUT using hydrated Ar (2.3 MGy-225 MGy).

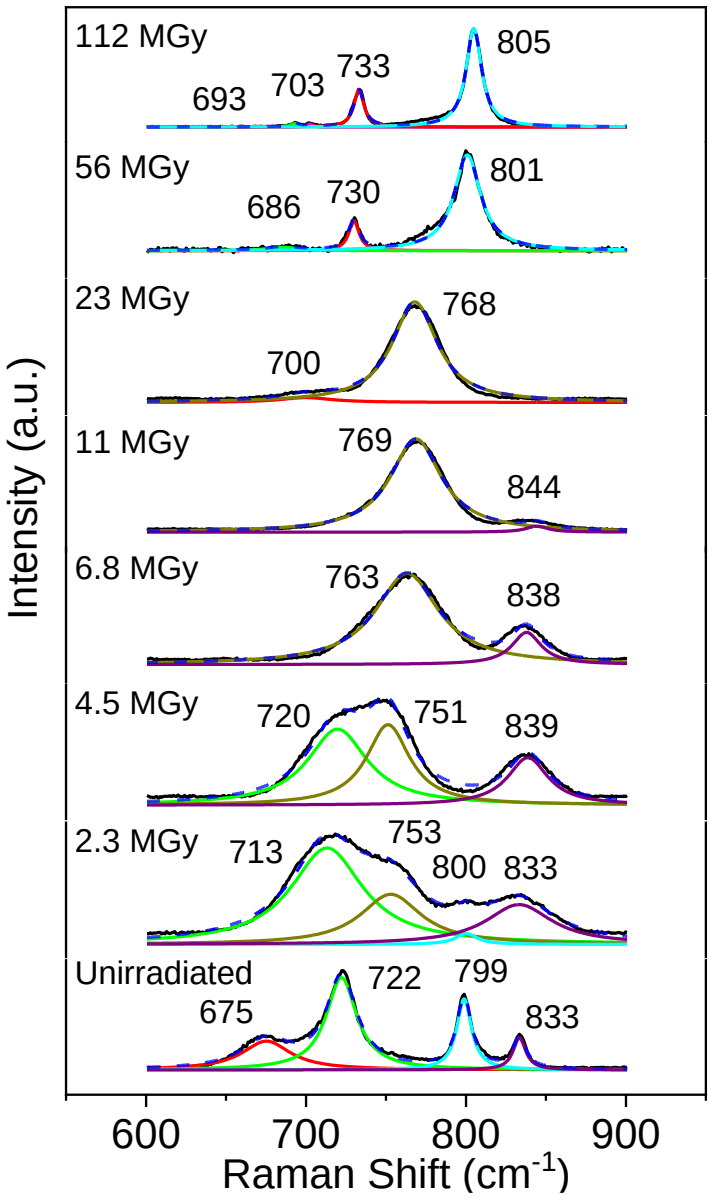

Figure S7. Static Raman fittings obtained from unirradiated and He-ion irradiated NaUT using hydrated Ar (2.3 MGy-112 MGy).

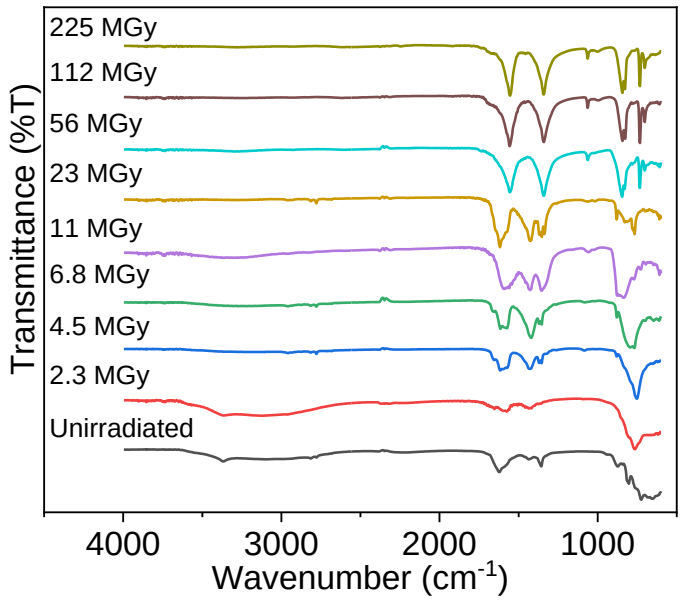

Figure S8. Infrared spectra obtained from unirradiated and He-ion irradiated NaUT using hydrated Ar (2.3 MGy-225 MGy).

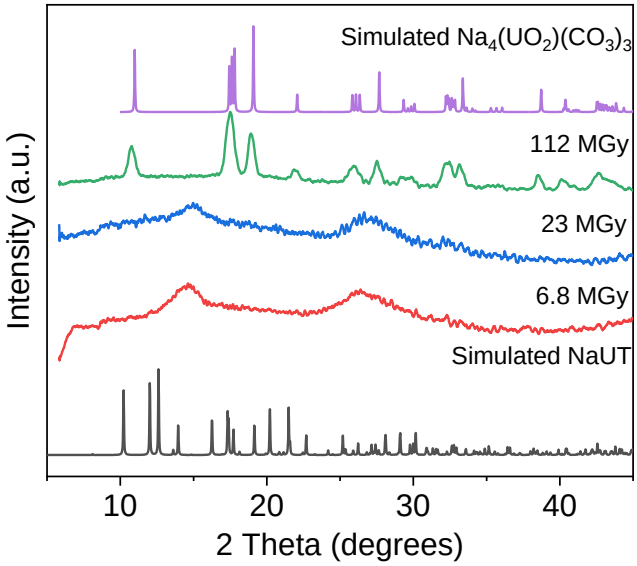

Figure S9. Powder X-ray diffraction pattern of He-ion irradiated NaUT using hydrated Ar to 6.8 MGy, 23 MGy, and 112 MGy with the simulated for NaUT and $Na_4(UO_2)(CO_3)_3$.

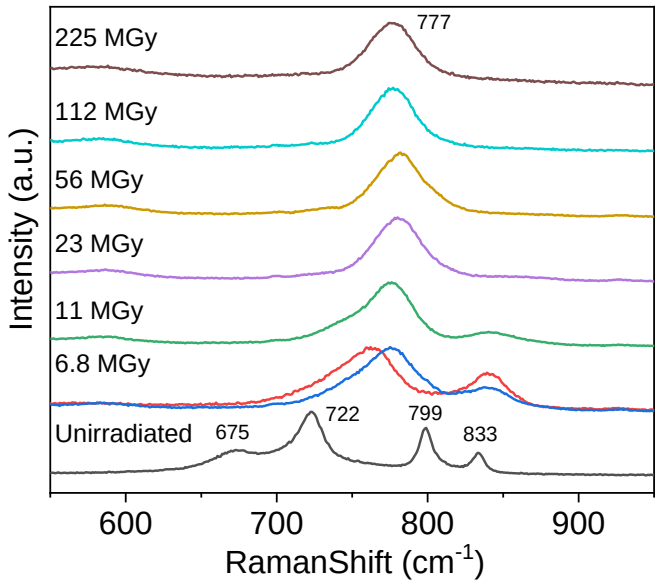

Figure S10. Static Raman spectra of unirradiated and He-ion irradiated NaUT (6.8 MGy-225 MGy) using a dry argon flow. Multiple lines at the same dose indicate different particles of the sample.

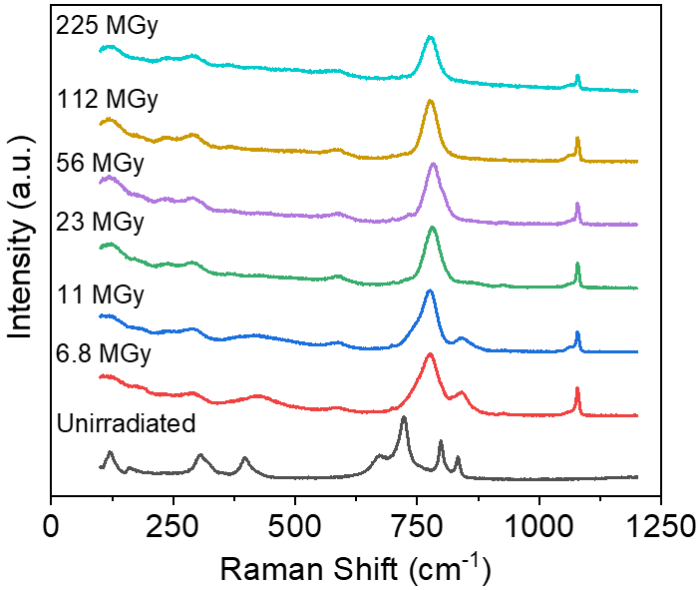

Figure S11. Extended Raman spectra of unirradiated and He-ion irradiated NaUT (6.8 MGy-225 MGy) using a dry Ar flow.

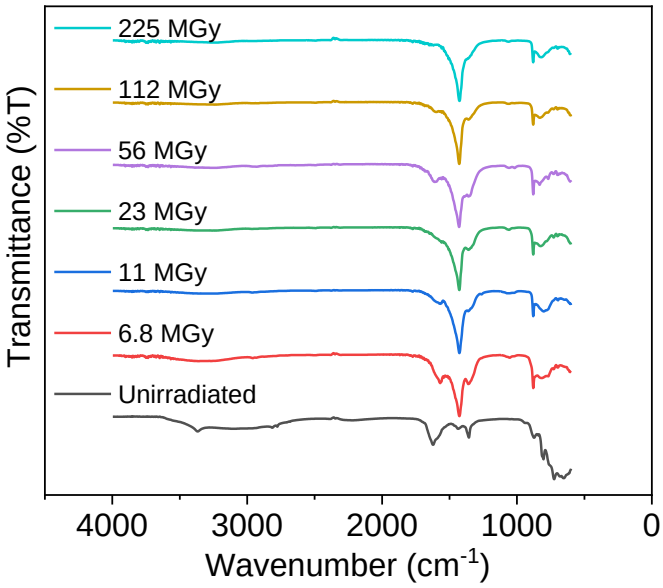

Figure S12. Infrared spectra of unirradiated and He-ion irradiated NaUT (6.8 MGy-225 MGy) using a dry Ar flow.

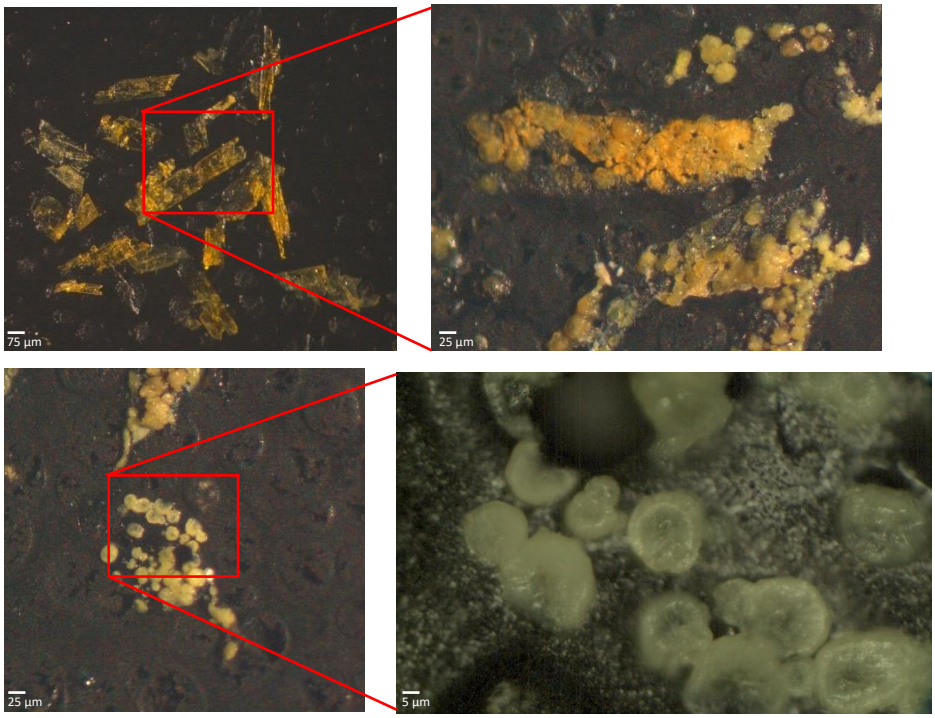

Figure S13. Microscope images of the blade crystal shape of the NaUT changes to the round crystal shape of the tricarbonate phase, cejkaite.

Table S1. Fittings for Raman spectra obtained from Unirradiated and γ-irradiated NaUT.

Results	**Unirradiated NaUT**	**1 MGy γ-irradiated NaUT**	**2 MGy γ-irradiated NaUT**	**3 MGy γ-irradaited NaUT**
Iterations	107	84	20	228
Convergence	1e-9	1e-9	1e-9	1e-9
Residual Sum of Squares (RSS)	2.58389e7	1.952910e6	2.619839e4	4.6687e4
Coefficient of Determination (R^2)	0.9877	0.9977	0.9973	0.9962
Peak location (cm^{-1})	679.90 ± 0.49 727.62 ± 0.12 803.45 ± 0.21 816.94 ± 0.94 839.01 ± 0.17	691.40 ± 0.18 714.52 ± 0.22 729.48 ± 0.37 764.58 ±0.56 804.17 ± 0.55 816.15 ± 1.06 838.16 ± 0.32 853 (restrained) 865.90 ± 0.30	692.72 ± 0.05 715.48 ± 0.07 764.68 ± 0.21 841.67 ± 0.77 865.75 ± 0.12 876.04 ± 0.21	717.16 ± 0.59 758.83 ± 1.45 776.35 ±0.72 863.96 ± 0.77 841.80 ± 0.28
Full-width half max (FWHM)	41.21 ± 1.76 25.59 ± 0.42 11.22 ± 0.77 20 ± 3.15 7.71 ± 0.60	13.30 ± 0.89 7.55 ± 1.05 60.45 ± 1.14 22.86 ± 2.57 4.37 ± 1.95 12.89 ± 4.16 32.33 (restrained) 10.20 ± 1.00	13.03 ± 0.16 18.30 ± 0.25 48.19 ± 0.84 28.60 ± 2.80 7.93 ± 0.47 9.44 ± 0.65	24.11 ± 2.54 42.87 ± 1.45 28.68 ± 2.41 8.03 ± 2.69 23.78 ± 1.03

Table S2. Fittings for Raman spectra obtained from Unirradiated and ^{4}He-irradiated NaUT.									
Results	**Unirradiated NaUT**	**2.3 MGy ^{4}He-irradiated NaUT**	**4.5 MGy ^{4}He-irradiated NaUT**	**6.8 MGy ^{4}He-irradiated NaUT**	**11 MGy ^{4}He-irradiated NaUT**	**23 MGy ^{4}He-irradiated NaUT**	**56 MGy ^{4}He-irradiated NaUT**	**112 MGy ^{4}He-irradiated NaUT**	**225 MGy ^{4}He-irradiated NaUT**
Iterations	16	31	300	19	105	36	23	14	15
Convergence	1e-9	1e-9	1e-9	1e-9	1e-9	1e-9	1e-9	1e-9	1e-9
Residual Sum of Squares (RSS)	3.4814e4	3.7979e4	2.93657e7	1.08492e5	2.01318e5	1.79242e5	1.54997e7	5.3443e4	2.35794e7
Coefficient of Determination (R^2)	0.9920	0.9944	0.9879	0.9862	0.99314	0.9900	0.9849	0.9934	0.9920
Peak location (cm^{-1})	675.23 ± 0.38 722.22 ± 0.09 798.88 ± 0.08 833.44 ± 0.15	713.16 ± 0.38 753.12 ± 0.57 800.28 ± 0.83 833.18 ± 0.58	719.70 ± 0.61 751.31 ± 0.38 838.71 ± 0.33	763.19 ± 0.18 837.92 ± 0.35	768.70 ± 0.11 844.35 ± 1.10	700.00 ± 2.81 768.01 ± 0.12	685.65 ± 2.87 729.97 ± 0.18 800.87 ± 0.09	639.17 ± 0.87 702.51 ± 0.83 733.10 ± 0.08 804.94 ± 0.04	689.01 ± 1.21 729.39 ± 0.09 801.52 ± 0.05
Full-width half max (FWHM)	36.96 ± 1.36 23.16 ± 0.30 11.20 ± 0.23 9.47 ± 0.47	54.43 ± 1.08 46.20 ± 2.14 16.55 ± 3.51 50.36 ± 1.93	45.30 ± 1.62 32.94 ± 1.15 30.76 ± 1.18	47.95 ± 0.68 22.32 ± 1.11	38.72 ± 0.38 16.66 ± 3.40	39.73 ± 9.71 34.10 ± 0.42	24.02 ± 9.54 7.71 ± 0.55 20.19 ± 0.30	6.44 ± 2.82 4.40 ± 2.71 7.57 ± 0.24 11.72 ± 0.12	18.95 ± 3.86 7.84 ± 0.27 12.87 ± 0.14